Journal of Zhejiang University-SCIENCE A (Applied Physics & Engineering) 2024 25(8):680-686
www.jzus.zju.edu.cn; www.springer.com/journal/11582
E-mail: jzus_a@zju.edu.cn

**Correspondence**

https://doi.org/10.1631/jzus.A2300276

Check for updates

# Enhancement in the $Hg^0$ oxidation efficiency and sulfur resistance of $CuCl_2$-modified $MnO_x$-$CeO_x$ nanorod catalysts

Shujie GAO[1], Yongjin HU[1], Zhichang JIANG[1], Xiaoxiang WANG[2], Dong YE[1]✉, Changxing HU[3]✉

[1]*College of Quality & Safety Engineering, China Jiliang University, Hangzhou 310018, China*
[2]*Key Laboratory of Biomass Chemical Engineering of Ministry of Education, Institute of Industrial Ecology and Environment, College of Chemical and Biological Engineering, Zhejiang University, Hangzhou 310027, China*
[3]*School of Mechatronics and Energy Engineering, Ningbo Tech University, Ningbo 315100, China*

**Abstract:** In this study, a series of $CuCl_2$-modified $MnO_x$-$CeO_x$ nanorods were synthesized for the oxidation of $Hg^0$. The addition of $CuCl_2$ resulted in an enhancement in the catalyst's $Hg^0$ oxidation ability, and $Hg^0$ oxidation efficiency reached >97% from 150 to 250 °C. In the $MnO_x$-$CeO_x$ catalysts, $Mn^{4+}$ played the role of the active species for $Hg^0$ oxidization, but in the $CuCl_2$-doped catalysts $Cl^-$ also contributed to $Hg^0$ oxidation, conferring the superior performance of these samples. The introduction of $SO_2$ led to a decrease in the availability of $Mn^{4+}$, and the $Hg^0$ oxidation efficiency of $MnO_x$-$CeO_x$ decreased from about 100% to about 78%. By contrast, $CuCl_2$-promoted samples maintained a $Hg^0$ oxidation efficiency of about 100% during the $SO_2$ deactivation cycle due to the high reactivity of $Cl^-$.

**Key words:** $Hg^0$ oxidation; $CuCl_2$ modification; $MnO_x$-$CeO_x$ nanorods; Sulfur resistance; Oxidation activity

## 1 Introduction

Mercury is recognized as one of the most dangerous pollutants of the environment and human beings owing to its characteristics of neurotoxicity and bioaccumulation (Baltrus et al., 2008; Jampaiah et al., 2019a). Coal combustion has been identified as the major anthropogenic source of mercury emissions (Ye et al., 2022b). In flue gas, mercury is generally present in the forms of particle-bound mercury ($Hg^p$), oxidized mercury ($Hg^{2+}$), and elemental mercury ($Hg^0$) (Ye et al., 2021). The former two species can be eliminated via wet flue gas desulfurization (WFGD) and dust removal units, while the high volatility and low solubility of $Hg^0$ make it difficult to be removed using existing pollution control devices (Chalkidis et al., 2019). Therefore, improving the efficiency of $Hg^0$ elimination is an important step towards effectively reducing mercury emissions.

✉ Dong YE, Richard32@126.com
Changxing HU, huchx@zju.edu.cn
Dong YE, https://orcid.org/0000-0001-8299-224X

Received May 22, 2023; Revision accepted July 24, 2023; Crosschecked Apr. 25, 2024; Online first June 14, 2024



Among various techniques for $Hg^0$ abatement, the catalytic oxidation of $Hg^0$ to $Hg^{2+}$ is gaining popularity owing to the high solubility of $Hg^{2+}$, which can be effectively removed by subsequent desulfurization systems, thereby facilitating the elimination of $Hg^0$ from flue gas (Wu et al., 2017). The catalyst activity is crucial to the effectiveness of removal of $Hg^0$ from the entire system. Some catalysts, such as $CeO_2$-$CoO_x$-$TiO_2$ (Li et al., 2020), $CeO_2$-$WO_3$/$TiO_2$ (Yang et al., 2017b), $MnO_x$-$CeO_2$/$TiO_2$ (Li et al., 2012), $MnO_x$-$CeO_x$/activated carbon (Wu et al., 2017), and $CuCl_2$-$CoO_x$/$TiO_2$-$CeO_2$ (Li et al., 2017) have shown promising prospects for $Hg^0$ elimination. The superior oxygen storage capacity of $CeO_2$ can optimize the physicochemical properties of other components in the catalysts through synergistic effects, which positively affect the formation of reactive oxygen species and accelerate the oxidation of $Hg^0$. Consequently, a satisfactory $Hg^0$ oxidation efficiency of >95% can be achieved within a certain temperature range.

Based on variable flue gas conditions in real coal-fired power plants (Liu et al., 2020), many of the aforementioned catalysts can actively operate in low-$Hg^0$-concentration working gas (tens of μg/m$^3$) (Table S1 of the electronic supplementary materials (ESM)).

However, their effectiveness in eliminating $Hg^0$ from high-$Hg^0$-content gases (hundreds of μg/m$^3$) is uncertain. Additionally, exposure to $SO_2$-containing flue gas can lead to the sulfation of active agents, resulting in the formation of inert metal sulfates that significantly interfere with the $Hg^0$ elimination process (Wang et al., 2014; Ma et al., 2019). Therefore, developing a catalyst that exhibits superior activity under $Hg^0$-rich and $SO_2$-containing conditions is an urgent task with practical significance.

In a previous study we discovered that $MnO_x$-$CeO_x$ nanorods exhibited a $Hg^0$ removal efficiency of >90% in simulated flue gas with an $Hg^0$ concentration of 350 μg/m$^3$ (Ye et al., 2023b). Compared with nanocube-shaped counterparts, samples with a nanorod micro-topology exhibited enhanced $Hg^0$ abatement capability. $CuCl_2$ is an active agent for $Hg^0$ oxidation, particularly in $SO_2$-containing flue gas. The active chlorine species produced from $Cl^-$ can facilitate $Hg^0$ oxidation reactions, which endow $CuCl_2$-containing catalysts with satisfactory activity in the presence or absence of $SO_2$ (Li et al., 2013; Liu et al., 2015). Given this knowledge, doping highly active $CuCl_2$ may simultaneously enhance the $Hg^0$ oxidation ability and $SO_2$ resistance of $MnO_x$-$CeO_x$ catalysts. This could be significant for reducing mercury emissions but is yet to be reported in the literature.

In this study, $CuCl_2$-promoted $MnO_x$-$CeO_x$ catalysts were prepared using a combination of hydrothermal and wet impregnation methods. The $Hg^0$ oxidation activity and $SO_2$-resistance of the catalysts series were investigated using virgin $MnO_x$-$CeO_x$ used as a reference. The catalytic physicochemical properties were characterized using transmission electron microscopy (TEM), X-ray diffraction (XRD), $N_2$-adsorption-desorption, and X-ray photoelectron spectroscopy (XPS), to understand the mechanisms behind the enhancement of $Hg^0$ oxidation capability and $SO_2$ tolerance.

## 2 Materials and methods

### 2.1 Chemicals

$Ce(NO_3)_3·6H_2O$ (analytical reagent (AR): ≥99.0%; 100 g), $Mn(NO_3)_2$ aqueous solution (mass fraction: 50%; AR: 49.0%–51.0%; 500 mL), NaOH (AR: ≥96.0%; 500 g), and $CuCl_2·2H_2O$ (AR: ≥99.0%; 100 g) were obtained from Sinopharm Chemical Reagent Co., Ltd. (China).

### 2.2 Catalyst preparation

$MnO_x$-$CeO_x$ nanorods were synthesized using the hydrothermal technique of Ye et al. (2023b). The resulting product was then dried overnight at 80 °C and calcined at 450 °C for 4 h. $CuCl_2$-modified $MnO_x$-$CeO_x$ nanorods were prepared via the wet-impregnation method (Ye et al., 2020). Finally, the sample was calcined at 450 °C for 4 h in air (Fig. S1). The samples were labeled based on the $CuCl_2$ loading amount. For instance, MC denotes the virgin $MnO_x$-$CeO_x$ mixed oxide, and 5C-MC refers to the $MnO_x$-$CeO_x$ catalyst modified with 5% $CuCl_2$.

### 2.3 Catalyst preparation

The catalytic performance of the catalyst series was tested in a fixed bed reactor. The working gas, with a total flow rate of 600 mL/min, comprised 5% $O_2$, 350 μg/m$^3$ $Hg^0$, 400 ppm (1 ppm=$1\times10^{-6}$) $SO_2$ (when used), and nitrogen gas ($N_2$). $Hg^0$ vapor was generated through a mercury permeation tube placed in a water bath at 50 °C. In each test, 60 mg of the catalyst was used, corresponding to a gas hourly space velocity of 600 L/(g·h). Because the $Hg^0$ removal unit was located between the air pre-heater and the dust removal device, the temperature of the flue gas was always <250 °C. Considering the variable operation loads in real power plants, we evaluated the catalyst $Hg^0$ oxidation ability within the temperature range of 150–250 °C. The inlet ($A_{in}$) and outlet ($A_{out}$) concentrations of $Hg^0$ were monitored using an online mercury analyzer. The $Hg^0$ removal efficiency ($\eta$) was determined by

$$\eta = \frac{A_{in} - A_{out}}{A_{in}} \times 100\%. \quad (1)$$

### 2.4 Characterization

The textural structure parameters of the catalyst series were investigated by $N_2$ adsorption characterization, using an ASAP 2460 Version 3.01 Surface Area and Porosimetry Analyzer from Micromeritics, USA. The crystal information of the catalyst series was determined by XRD using a PANalytical B. V. spectrometer from PANalytical B.V., the Netherlands. The scan range was set as 10°–90° and the step size was 0.003°. The micro-topological structures of the investigated samples were observed using an FEI Tecnai F20

TEM from FEI, USA. The valence state of each element was determined by XPS using an ESCALab220i-XL electron spectrometer from VG Scientific, USA. The C 1s line at 284.6 eV was used for the binding energy calibration.

## 3 Results and discussion

### 3.1 Transmission electron microscopy and X-ray diffraction analysis

The micro-topological structures of the serial $CuCl_2$-promoted catalysts are shown in Fig. 1. The virgin MC appeared as nanorods with an aspect ratio of 20–40. After $CuCl_2$ modification, rod-shaped products with a relatively low aspect ratio of <10 were observed, which were attributed to the grinding behavior during the catalyst preparation stage. Fig. 1e illustrates the crystal structures of the catalyst, showing XRD diffraction peaks identical to those of fluorite $CeO_2$, indicating that the introduced $CuCl_2$ existed in an amorphous state on the $MnO_x$-$CeO_x$ surfaces.

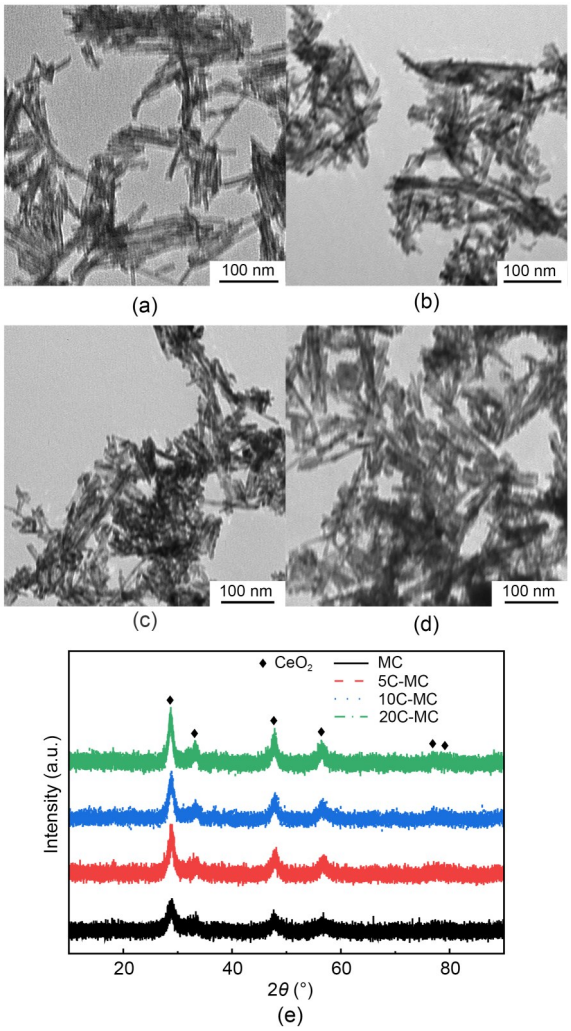


**Fig. 1 TEM images: (a) MC; (b) 5C-MC; (c) 10C-MC; (d) 20C-MC; (e) XRD patterns of the catalyst series. MC: virgin $MnO_x$-$CeO_x$ mixed oxide; 5C-MC, 10C-MC, and 20C-MC: $MnO_x$-$CeO_x$ catalysts modified with 5%, 10%, and 20% $CuCl_2$, respectively**

### 3.2 $N_2$-adsorption-desorption analysis

The $N_2$-adsorption-desorption isotherms of the catalyst series are shown in Fig. S2a. The $N_2$ adsorption value for all the samples showed a steep increase at a relative pressure region of $P/P_0$>0.8. The appearance of H3-typed hysteresis loops confirmed the presence of slit-like mesoporous structures in these catalysts (Sing, 1985). Additionally, a relatively broad pore size distribution was obtained for all the catalysts based on the results in Fig. S2b. The specific surface area, average pore diameter, and total pore volume of the catalyst series are shown in Table 1. After 5% $CuCl_2$ was doped, the specific surface area of the catalysts decreased by about 30%. As the loading amount of $CuCl_2$ increased to 10%, the specific surface area decreased to 44 $m^2/g$, which was 44% lower than that of the virgin MC nanorods. Further increases in the $CuCl_2$ doping showed negligible variations in the specific surface area of the catalysts. This behavior slightly interfered with the catalyst-reactant interaction and in turn had significant impacts on the $Hg^0$ oxidation reactions (Ye et al., 2023b).

**Table 1 Specific surface area, average pore diameter, and total pore volume of the catalyst series**

| Sample | Specific surface area ($m^2/g$) | Average pore diameter (nm) | Pore volume ($cm^3/g$) |
|---|---|---|---|
| MC | 78 | 17.2 | 0.50 |
| 5C-MC | 53 | 22.6 | 0.44 |
| 10C-MC | 44 | 21.0 | 0.35 |
| 20C-MC | 43 | 20.8 | 0.31 |

### 3.3 X-ray photoelectron spectroscopy analysis

The surface atom environment of the catalyst series was investigated using the XPS technique. In the case of manganese (Mn) atoms, the curve-fitted two sub-bands at about 645 and about 642 eV were successively evaluated with $Mn^{4+}$ and $Mn^{3+}$, respectively (Fig. S3a) (Ye et al., 2023a). The doping of 5% $CuCl_2$

led to a decrease in the relative content of $Mn^{4+}$ from about 24.4% to about 22.1%. As the $CuCl_2$ loading amount increased, this value steadily decreased to 18.2% (Table 2). The change was attributed to interactions between the existing Mn species and the loaded $CuCl_2$, which subsequently altered the atom environment of Mn. Similarly, the doping of $CuCl_2$ also contributed to a decrease in the content of $Ce^{4+}$ from 85.5% to 82.1%. The photoelectron peaks were centered at about 916, 907, 900, 898, 888, and 882 eV (Fig. S3b) (Jampaiah et al., 2019b). The results indicated that extraneous $Cl^-$ interacted with $Ce^{4+}$ species to form $CeCl_3$-like compounds, leading to an increase in the relative concentration of $Ce^{3+}$ (Jiang et al., 2018). In the case of the copper (Cu) atoms, deconvolution of the XPS spectra revealed three sub-peaks (Fig. 2a). The peak with a binding energy of about 628.2 eV corresponds to $Cu^+$, while those in the higher binding energy region were revealed by the presence of $Cu^{2+}$ (Zhou et al., 2018). These findings further confirmed the interactions between $CuCl_2$ and $MnO_x$ or $CeO_x$. Notably, the relative content of $Cu^+$ decreased from 16.9% to 7.2% as the amount of $CuCl_2$ increased, indicating that the decreased ratio of $CuCl_2$ strongly interacted with $MnO_x$-$CeO_x$ binary oxide (Ji et al., 2016). Fig. 2b shows the Cl 2p spectra of the serial samples. The resulting two sub-bands were attributed to the spin-orbit splitting of Cl $2p_{1/2}$ and Cl $2p_{3/2}$, confirming the presence of chloride species in the form of $Cl^-$ over the catalysts (Zhou et al., 2018).

**Table 2 XPS data of the catalyst series**

| Sample | Relative content (%) | | |
|---|---|---|---|
| | $Mn^{4+}$ | $Ce^{3+}$ | $Cu^+$ |
| MC | 24.4 | 14.5 | – |
| 5C-MC | 22.1 | 16.0 | 16.9 |
| 10C-MC | 20.9 | 17.4 | 14.1 |
| 20C-MC | 18.2 | 17.9 | 7.2 |

### 3.4 Performance results

Fig. 3 shows the activity results of the examined catalysts. The virgin $MnO_x$-$CeO_x$ exhibited about 100% $Hg^0$ removal efficiency at 150 °C. As the reaction temperature increased, the $Hg^0$ removal efficiency decreased, suggesting that higher temperatures significantly influenced the $Hg^0$ oxidation reactions. The trend was attributed to interference in the adsorption of $Hg^0$, leading to insufficient reactant availability for the subsequent oxidation stage and finally resulting in an inhibited high-temperature $Hg^0$ oxidation ability (Yang et al., 2011; Ye et al., 2022a). With the doping of $CuCl_2$, the catalyst $Hg^0$ removal efficiency maintained about 97% throughout the investigated temperature range, indicating an enhancement in the $Hg^0$ removal capability of $CuCl_2$-promoted catalysts.

Considering that $SO_2$ is typically present in real coal-fired flue gas, investigating its influence on

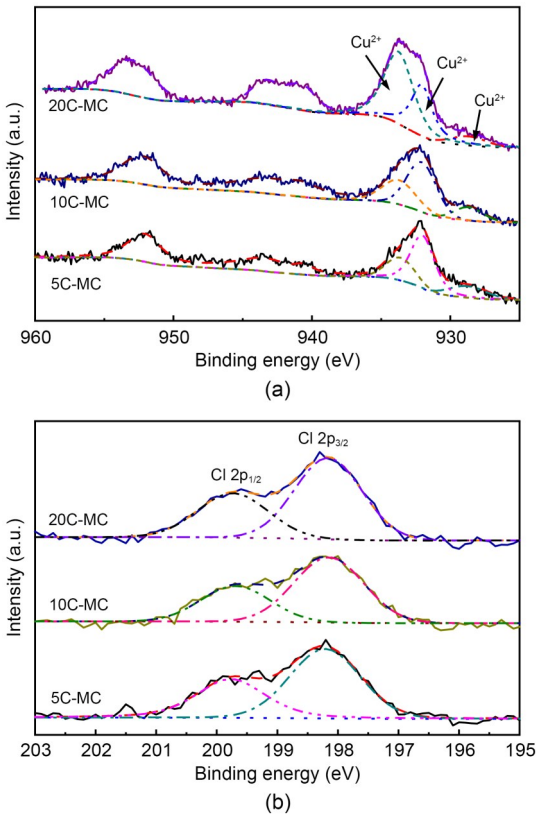


**Fig. 2 XPS spectra: (a) Cu 2p; (b) Cl 2p. References to color refer to the online version of this figure**

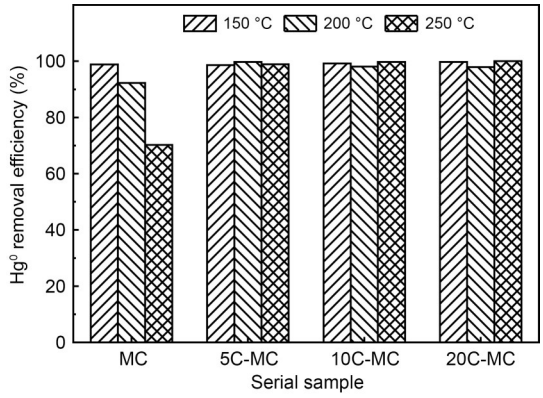


**Fig. 3 $Hg^0$ removal efficiency of the catalyst series**

catalyst performance is essential. An $Hg^0$ removal efficiency of MC and 5C-MC of about 98% during the 5-h reaction cycle in the absence of $SO_2$ was observed, indicating the satisfactory stability of the two catalysts (Fig. 4). In this study, $SO_2$ was introduced into the reaction system, and the $Hg^0$ removal efficiency of MC steadily decreased over the reaction time. These findings confirmed that $SO_2$ had an inhibitory effect on the $Hg^0$ oxidation reactions, which was explained by the competitive adsorption of $SO_2$ and $Hg^0$ onto the catalyst active sites and the formation of inert metal sulfates (Galloway et al., 2018). In contrast, the $CuCl_2$-promoted catalyst appeared to be resistant to sulfur deactivation owing to the negligible decrease in the $Hg^0$ removal efficiency after 5 h of exposure to the $SO_2$-containing flue gas. The results indicated that the $CuCl_2$-doped $MnO_x$-$CeO_x$ catalysts have satisfactory sulfur resistance.

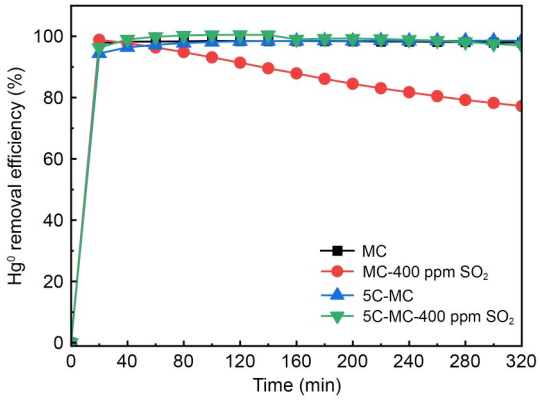


**Fig. 4 $SO_2$-tolerance of MC and 5C-MC catalysts**

Considering the catalytic oxidation reaction of $Hg^0$ was similar to the increased valence state of the Hg atoms from 0 to +2, the catalyst redox properties played a significant role in this process. According to the XPS results, $Mn^{4+}$ was the active species in the virgin $MnO_x$-$CeO_x$ nanorods (Fig. S4 and Table 3). After doping with $CuCl_2$, in addition to $Mn^{4+}$, the $Cl^-$ anion contributed to the oxidation of $Hg^0$, as shown by the decrease in the Cl content of the spent MC sample (Table 3 and Fig. S5). Under the action of oxygen and high-valence-state metal cations, $Cl^-$ was activated into active chlorine species ($Cl^*$), which exhibited superior reactivity and accelerated the $Hg^0$ oxidation process (Fig. 5) (Li et al., 2017; Yang et al., 2017a). Although the addition of $CuCl_2$ led to a decrease in the specific surface area and the content of active

**Table 3 Measured data of the experiments in six states**

| Sample | Relative content (%) | | | Cl/(Mn+Ce+Cu)* |
|---|---|---|---|---|
| | $Mn^{4+}$ | $Ce^{3+}$ | $Cu^{2+}$ | |
| MC | 24.4 | 14.5 | – | – |
| Spent MC (without $SO_2$) | 20.0 | 15.0 | – | – |
| Spent MC (with $SO_2$) | 13.9 | 22.3 | – | – |
| 5C-MC | 22.1 | 16.0 | 16.9 | 0.14 |
| Spent 5C-MC (without $SO_2$) | 18.2 | 16.1 | 16.6 | 0.11 |
| Spent 5C-MC (with $SO_2$) | 17.0 | 18.7 | 16.4 | 0.04 |

* Ratio of Mn and metal cations (Cu, Mn, and Ce)

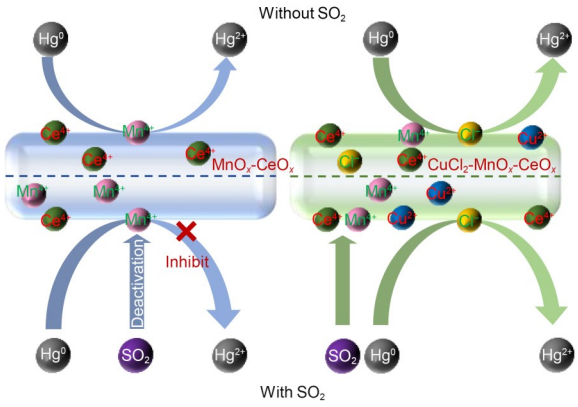


**Fig. 5 Mechanisms of the enhanced $Hg^0$ oxidation capability and $SO_2$-tolerance of $CuCl_2$-doped $MnO_x$-$CeO_x$ catalysts. References to color refer to the online version of this figure**

$Mn^{4+}$, this negative effect was more than offset by the promotional impact of the introduced highly active $Cl^-$. Consequently, the $CuCl_2$-doped catalysts had an enhanced $Hg^0$ oxidation ability (Ye et al., 2023b).

Furthermore, in the presence of $SO_2$ in the reaction systems, apart from the main reaction of $Hg^0$ oxidation, a side reaction involving the formation of inert metal sulfates occurred (Zhang AC et al., 2015; Zhang D et al., 2018). Thus, the performance of the catalyst in the $SO_2$-containing flue gas was related to the dominance of either the main reaction or the side reaction (Zhang et al., 2018). According to the XPS results in Table 3, after the reaction in the $SO_2$-containing flue gas, a decrease in the content of $Mn^{4+}$ was observed compared with the sample without $SO_2$ poisoning, indicating the formation of $MnSO_4$-like compounds on $MnO_x$-$CeO_x$ surfaces (Zhou et al., 2022). This decrease reduced the availability of active species and subsequently inhibited the oxidation stage of $Hg^0$, which contributed to a decreased $Hg^0$ oxidation efficiency in the presence of $SO_2$. The $CuCl_2$-doped sample also showed a decrease in the content of $Mn^{4+}$ after

the $SO_2$ deactivation cycle compared with the catalyst after $Hg^0$ oxidation in the clean working gas, indicating the occurrence of a side reaction resulting in the formation of inert sulfate salts. Thus, $Mn^{4+}$ contributed slightly to $Hg^0$ oxidation (Li et al., 2017). However, the added $Cl^-$ compensated for this through its significant contribution to the $Hg^0$ oxidation reaction (Fig. 5). Subsequently, the consumption of $Cl^-$ was accelerated, resulting in a lower amount of chlorine species remaining on the catalyst surface (Table 3). Thus, the presence of $Cl^-$ played a significant role in obtaining the relatively high $Hg^0$ oxidation efficiency in the absence or presence of $SO_2$.

From an economic perspective, the improved $Hg^0$ oxidation efficiency resulting from the addition of $CuCl_2$ indicates that a reduced amount of catalyst was needed to meet the $Hg^0$ emission standards. Furthermore, the enhanced $SO_2$-tolerant ability indicates that the catalysts' lifespan was prolonged, reducing the need for replacements and lowering operational costs. These advantages provide guidelines for the effective reduction of mercury emissions from flue gas with high $Hg^0$ content (hundreds of μg/m$^3$) and a significant amount of $SO_2$ (hundreds of ppm). This method is also beneficial for achieving the goal of effectively reducing mercury emissions from industrial sources.

## 4 Conclusions

In this study, we successfully modified $MnO_x$-$CeO_x$ nanorods with $CuCl_2$ to simultaneously improve the $Hg^0$ oxidation capability and $SO_2$-tolerance of the catalysts. The following conclusions were drawn:

1. The addition of $CuCl_2$ enhances the catalyst's $Hg^0$ oxidation capability, with $Hg^0$ oxidation efficiency at >97% throughout the investigated temperature range for $CuCl_2$-doped samples. In the presence of 400 ppm $SO_2$, the $Hg^0$ oxidation efficiency of $MnO_x$-$CeO_x$ steadily decreased from about 100% to about 78% after 320 min, whereas the $CuCl_2$-doped catalysts maintained about 100% $Hg^0$ oxidation efficiency during the $SO_2$ deactivation cycle.

2. For the $MnO_x$-$CeO_x$ catalyst, $Mn^{4+}$ served as the active species for $Hg^0$ oxidization. However, with the addition of $CuCl_2$, the introduced $Cl^-$ with high reactivity was mainly responsible for accelerating the oxidation of $Hg^0$, resulting in enhanced $Hg^0$ oxidation capability of the $CuCl_2$-doped catalysts.

3. In the presence of $SO_2$, the decreased availability of $Mn^{4+}$ largely explained the decreased $Hg^0$ oxidation efficiency of the $MnO_x$-$CeO_x$ catalyst. However, with the addition of $CuCl_2$, $Cl^-$ ensured the effective oxidation of $Hg^0$, thereby maintaining a high $Hg^0$ oxidation efficiency during the $SO_2$ deactivation cycle.

## Acknowledgments

This work is supported by the Zhejiang Provincial Natural Science Foundation of China (No. LQ22E060003), the General Research Projects of Zhejiang Provincial Department of Education in 2023 (No. Y202353660), and the Public Welfare Science and Technology Project of Ningbo City (No. 202002N3105), China.

## Author contributions

Shujie GAO designed the research. Yongjin HU and Zhichang JIANG processed the corresponding data. Dong YE wrote the first draft of the manuscript. Xiaoxiang WANG helped to organize the manuscript. Changxing HU revised and edited the final version.

## Conflict of interest

Shujie GAO, Yongjin HU, Zhichang JIANG, Xiaoxiang WANG, Dong YE, and Changxing HU declare that they have no conflict of interest.

## References

Baltrus JP, Granite EJ, Stanko DC, et al., 2008. Surface characterization of $Pd/Al_2O_3$ sorbents for mercury capture from fuel gas. *Main Group Chemistry*, 7(3):217-225. https://doi.org/10.1080/10241220802509432

Chalkidis A, Jampaiah D, Hartley PG, et al., 2019. Regenerable α-$MnO_2$ nanotubes for elemental mercury removal from natural gas. *Fuel Processing Technology*, 193:317-327. https://doi.org/10.1016/j.fuproc.2019.05.034

Galloway B, Royko M, Sasmaz E, et al., 2018. Mercury oxidation over Cu-SSZ-13 catalysts under flue gas conditions. *Chemical Engineering Journal*, 336:253-262. https://doi.org/10.1016/j.cej.2017.11.163

Jampaiah D, Chalkidis A, Sabri YM, et al., 2019a. Low-temperature elemental mercury removal over $TiO_2$ nanorods-supported $MnO_x$-$FeO_x$-$CrO_x$. *Catalysis Today*, 324:174-182. https://doi.org/10.1016/j.cattod.2018.11.049

Jampaiah D, Chalkidis A, Sabri YM, et al., 2019b. Role of ceria in the design of composite materials for elemental mercury removal. *The Chemical Record*, 19(7):1407-1419. https://doi.org/10.1002/tcr.201800161

Ji PD, Gao X, Du XS, et al., 2016. Relationship between the molecular structure of $V_2O_5/TiO_2$ catalysts and the reactivity of $SO_2$ oxidation. *Catalysis Science & Technology*, 6(4):1187-1194. https://doi.org/10.1039/c5cy00867k

Jiang Y, Lu MY, Liu SJ, et al., 2018. Deactivation by HCl of $CeO_2$-$MoO_3/TiO_2$ catalyst for selective catalytic reduction

of NO with $NH_3$. *RSC Advances*, 8(32):17677-17684. https://doi.org/10.1039/c8ra00280k

Li HH, Wang SK, Wang X, et al., 2017. Activity of $CuCl_2$-modified cobalt catalyst supported on Ti-Ce composite for simultaneous catalytic oxidation of $Hg^0$ and NO in a simulated pre-sco process. *Chemical Engineering Journal*, 316:1103-1113. https://doi.org/10.1016/j.cej.2017.02.052

Li HH, Zhang JD, Cao YX, et al., 2020. Enhanced activity and $SO_2$ resistance of co-modified $CeO_2$-$TiO_2$ catalyst prepared by facile co-precipitation for elemental mercury removal in flue gas. *Applied Organometallic Chemistry*, 34(4):e5463. https://doi.org/10.1002/aoc.5463

Li HL, Wu CY, Li Y, et al., 2012. Superior activity of $MnO_x$-$CeO_2$/$TiO_2$ catalyst for catalytic oxidation of elemental mercury at low flue gas temperatures. *Applied Catalysis B: Environmental*, 111-112:381-388. https://doi.org/10.1016/j.apcatb.2011.10.021

Li X, Liu ZY, Kim J, et al., 2013. Heterogeneous catalytic reaction of elemental mercury vapor over cupric chloride for mercury emissions control. *Applied Catalysis B: Environmental*, 132-133:401-407. https://doi.org/10.1016/j.apcatb.2012.11.031

Liu H, Chang L, Liu WJ, et al., 2020. Advances in mercury removal from coal-fired flue gas by mineral adsorbents. *Chemical Engineering Journal*, 379:122263. https://doi.org/10.1016/j.cej.2019.122263

Liu ZY, Li X, Lee JY, et al., 2015. Oxidation of elemental mercury vapor over γ-$Al_2O_3$ supported $CuCl_2$ catalyst for mercury emissions control. *Chemical Engineering Journal*, 275:1-7. https://doi.org/10.1016/j.cej.2015.04.022

Ma YP, Mu BL, Zhang XJ, et al., 2019. Graphene enhanced Mn-Ce binary metal oxides for catalytic oxidation and adsorption of elemental mercury from coal-fired flue gas. *Chemical Engineering Journal*, 358:1499-1506. https://doi.org/10.1016/j.cej.2018.10.150

Sing KSW, 1985. Reporting physisorption data for gas/solid systems with special reference to the determination of surface area and porosity. *Pure and Applied Chemistry*, 57(4): 603-619. https://doi.org/ 10.1351/pac198557040603

Wang PY, Su S, Xiang J, et al., 2014. Catalytic oxidation of $Hg^0$ by $MnO_x$-$CeO_2$/γ-$Al_2O_3$ catalyst at low temperatures. *Chemosphere*, 101:49-54. https://doi.org/10.1016/j.chemosphere.2013.11.034

Wu J, Zhao Z, Huang TF, et al., 2017. Removal of elemental mercury by Ce-Mn co-modified activated carbon catalyst. *Catalysis Communications*, 93:62-66. https://doi.org/10.1016/j.catcom.2017.01.016

Yang SJ, Guo YF, Yan NQ, et al., 2011. Elemental mercury capture from flue gas by magnetic Mn-Fe spinel: effect of chemical heterogeneity. *Industrial & Engineering Chemistry Research*, 50(16):9650-9656. https://doi.org/10.1021/ie2009873

Yang YJ, Liu J, Zhang BK, et al., 2017a. Density functional theory study on the heterogeneous reaction between $Hg^0$ and HCl over spinel-type $MnFe_2O_4$. *Chemical Engineering Journal*, 308:897-903. https://doi.org/10.1016/j.cej.2016.09.128

Yang YJ, Liu J, Zhang BK, et al., 2017b. Experimental and theoretical studies of mercury oxidation over $CeO_2$-$WO_3$/$TiO_2$ catalysts in coal-fired flue gas. *Chemical Engineering Journal*, 317:758-765. https://doi.org/10.1016/j.cej.2017.02.060

Ye D, Wang XX, Liu H, et al., 2020. Insights into the effects of sulfate species on CuO/$TiO_2$ catalysts for $NH_3$-SCR reactions. *Molecular Catalysis*, 496:111191. https://doi.org/10.1016/j.mcat.2020.111191

Ye D, Wang XX, Wang RX, et al., 2021. Recent advances in $MnO_2$-based adsorbents for mercury removal from coal-fired flue gas. *Journal of Environmental Chemical Engineering*, 9(5):105993. https://doi.org/10.1016/j.jece.2021.105993

Ye D, Wang RX, Wang XX, et al., 2022a. Improvement in the $Hg^0$ removal performance of $CeO_2$ by modifying with CuO. *Applied Surface Science*, 579:152200. https://doi.org/10.1016/j.apsusc.2021.152200

Ye D, Wang XX, Wang RX, et al., 2022b. Review of elemental mercury ($Hg^0$) removal by CuO-based materials. *Journal of Zhejiang University-SCIENCE A (Applied Physics & Engineering)*, 23(7):505-526. https://doi.org/10.1631/jzus.A2100627

Ye D, Hu YJ, Jiang ZC, et al., 2023a. Mechanistic investigation on $Hg^0$ capture over $MnO_x$ adsorbents: effects of the synthesis methods. *Journal of Zhejiang University-SCIENCE A (Applied Physics & Engineering)*, 24(1):80-90. https://doi.org/10.1631/jzus.A2200388

Ye D, Gao SJ, Wang YL, et al., 2023b. New insights into the morphological effects of $MnO_x$-$CeO_x$ binary mixed oxides on $Hg^0$ capture. *Applied Surface Science*, 613:156035. https://doi.org/10.1016/j.apsusc.2022.156035

Zhang AC, Zhang ZH, Lu H, et al., 2015. Effect of promotion with Ru addition on the activity and $SO_2$ resistance of $MnO_x$-$TiO_2$ adsorbent for $Hg^0$ removal. *Industrial & Engineering Chemistry Research*, 54(11):2930-2939. https://doi.org/10.1021/acs.iecr.5b00211

Zhang D, Hou LA, Chen GY, et al., 2018. Cr doping $MnO_x$ adsorbent significantly improving $Hg^0$ removal and $SO_2$ resistance from coal-fired flue gas and the mechanism investigation. *Industrial & Engineering Chemistry Research*, 57(50):17245-17258. https://doi.org/10.1021/acs.iecr.8b04857

Zhou ZJ, Liu XW, Hu YC, et al., 2018. An efficient sorbent based on $CuCl_2$ loaded $CeO_2$-$ZrO_2$ for elemental mercury removal from chlorine-free flue gas. *Fuel*, 216:356-363. https://doi.org/10.1016/j.fuel.2017.11.134

Zhou ZJ, Liu L, Liu XW, et al., 2022. Catalytic oxidation of $Hg^0$ over Mn-doped $CeO_2$-$ZrO_2$ solid solution and $MnO_x$/$CeO_2$-$ZrO_2$ supported catalysts: characterization, catalytic activity and $SO_2$ resistance. *Fuel*, 310:122317. https://doi.org/10.1016/j.fuel.2021.122317

## Electronic supplementary materials

Table S1, Figs. S1–S5